**Educational Administration: Theory and Practice**
2024, 30(10), 744-746
ISSN: 2148-2403
https://kuey.net/

Research Article

# Macular Degeneration Diagnosis Using OLQCT Preprocessing, Fuzzy Segmentation, And BPN Classifier

J. Jency[1*] S. Shunmugan[2]

[1]Research Scholar, Department of Computer Science, S.T. Hindu College, Nagercoil, Affiliated to Manonmaniam Sundaranar University, Tirunelveli, India. jencysekar1995@gmail.com
[2]Associate Professor, Department of Computer Science and Applications, S.T. Hindu College, Nagercoil, Affiliated to Manonmaniam Sundaranar University, Tirunelveli, India. shunsthc@gmail.com

**Citation:** J. Jency, et al (2024), Macular Degeneration Diagnosis Using OLQCT Preprocessing, Fuzzy Segmentation, And BPN Classifier, *Educational Administration: Theory and Practice*, 30(10), 744-746
Doi: 10.53555/kuey.v30i10.9800

**ARTICLE INFO**

**ABSTRACT**

Macular degeneration is a condition that impairs central vision. It damages the macula which is the part of the retina that is responsible for sharp, straight-ahead vision. Age-related Macular Degeneration (AMD) is a specific age-related form of macular degeneration disease. AMD is a leading cause of vision impairment worldwide, necessitating early and accurate diagnosis for effective treatment. This research proposes an advanced method namely, '*Macular Degeneration Diagnosis using OLQCT Preprocessing, Fuzzy Segmentation, and BPN classifier (MDD_OFB)*', for AMD diagnosis by combining 'OLQCT preprocessing', 'fuzzy segmentation', and 'Back Propagation Neural network (BPN) classifier'. The new contribution of this work is a new preprocessing module, namely 'Macular region preprocessing using OD elimination, Log enhancement, Quantization, Contrast stretching and Thresholding (OLQCT)' which enhances the image quality of the macula region. Fuzzy segmentation is used to segment both the macula region and the wet macular region. The BPN classifier further classifies the extracted-features to diagnose the AMD accurately. Another contribution to this research is the new framework that is designed to integrate the four modules such as OLQCT preprocessing, dual-stage FCM segmentation, feature extraction, and BPN classifier. The proposed MDD_OFB method utilizes the KFI_DB, STARE_DB, and RFMI-DB datasets, ensuring robustness across diverse cases. Experimental results demonstrate an enhanced diagnostic performance, with significant improvements in Precision, Average Accuracy, Dice Coefficient, etc., when compared to existing methods. This proposed method enhances the accuracy by 2.056% than the second-best MD_MLC method. This integrated approach offers an advanced tool for early AMD detection, providing significant advantages in clinical practices. The proposed system ensures higher accuracy, lesser time consumption, reliability, and efficiency for AMD diagnosis.

**Keywords:** Macular Degeneration, OLQCT Preprocessing, Fuzzy Segmentation, Back Propagation Neural Network, Fundus Imaging, Image Processing, Diagnosis System.

## 1. Introduction

The eye-fundus image is the most often used modality for examining the human eye. It is crucial for the identification and management of numerous eye illnesses. It provides a clear study of the structure of the macula, perhaps revealing the presence of macula-related eye disease [1].

The macula is a small but incredibly important component of the anatomy of the eye. It is located in the middle of the retina in the back of the eye. The macula is a tiny structure in the human eye, measuring only 5 millimeters in diameter, but it is very important. It is in charge of center vision, which enables us to clearly perceive little details when identifying traffic signs, human faces, and words on a page. In addition, the macula plays an aspect in color vision, sense of clarity, and sharpness. For routine tasks requiring detailed vision, the macula's health is important.

Age-related Macular Degeneration is one of the disorders in the macula that can damage the macula and cause considerable loss of vision. AMD is a progressive ocular disease that mainly affects the elderly. AMD is the primary cause of vision loss in adults 50 years of age and beyond. It comes in two primary forms: wet AMD (neovascular) and dry AMD (atrophic). Wet AMD is common but more severe, and frequently results in rapid vision loss, whereas dry AMD proceeds more slowly and is more prevalent. AMD can seriously impede daily

activities such as reading, driving, and facial recognition. Regular eye exams are essential for anyone at risk of AMD because, while there is currently no treatment. Early detection and management techniques can help to reduce the disease's progression. The symptoms of AMD can differ according to the kind and phase of the illness. Typical symptoms consist of (i) Blurred central vision, (ii) Dark or Empty areas in vision, (iii) Distorted vision, (iv) Colors appearing less bright, (v) Sudden loss of central vision, etc., [2], [3], [4].
In digital image processing and computer vision, image segmentation is a method that divides a digital image into distinct parts or segments for evaluation. Macula segmentation is a critical issue in medical image processing in the field of ophthalmology. Its main objective is to precisely locate and extract the macula region from fundus images, which is important for tracking and diagnosing conditions that affect the eyes, like Diabetic Macular Edema (DME) and AMD [5], [6]. The computerized AMD diagnosis is a task that detects age-related macular degeneration disease through digital approaches using fundus images. It is a difficult process because of the complexity of retinal images, which include the macula region's low contrast, size and shape fluctuations, a number of overlapping structures, and distortions caused by diseases. These characteristics offer major challenges to diagnosing AMD, which requires the use of sophisticated image processing and machine learning techniques to increase the accuracy of clinical application [7], [8]. The existing systems in AMD diagnosis suffer from low accuracy, high runtime, and high false acceptance. Hence, this research focuses on an automatic AMD diagnosis method 'Macular Degeneration Diagnosis using OLQCT Preprocessing, Fuzzy Segmentation, and BPN Classifier (MDD_OFB)', to solve the drawbacks of existing methods. The main contributions of the proposed system are as follows:

- New preprocessing module, namely 'Macular region preprocessing using OD elimination, Log enhancement, Quantization, Contrast stretching and Thresholding (OLQCT)' to enhance the macula region to adapt to the upcoming macula region-oriented segmentation process.
- Design of novel framework that integrates the components such as (i) OLQCT preprocessing, (ii) Dual stage fuzzy c means segmentation integrated with both macula region segmentation and Wet Macular segmentation, (iii) Feature extraction, and (iv) BPN classifier.

The following research article explores the related works regarding the proposed work in Section 2, proposed methodology in Section 3, experimental results in Section 4, discussion in Section 5, and conclusion in Section 6.

## 2. Related Works

Tobin et al. [9] described an automatic identification of the optic nerve and the macula's location using digital red-free fundus photography. This method works based on precisely segmenting the retina's vasculature, which is followed by the identification of spatial features that characterize the density, average thickness, and average orientation of the vasculature concerning the optic nerve's location. After determining the location of the optic nerve, the macula is localized by employing a geometric model of the vasculature to identify the retina's horizontal raphe. The flaw of this method is that it fails to correctly identify the macula position. Niemeijer et al. [10] exposed the OD, macula, and vascular arch which are the three main anatomical components that may be automatically identified in color fundus images. A single-point distribution model that includes points on each structure is fitted to the image in order to identify these structures. Both left and right optic disc and macula-focused images can be processed using this method. This system determines the accurate location of the model points using a cost function that is based on a combination of local and global data. A limitation of a global approach is that it can lead to failures in other areas if one area fails.

Giancardo et al. [11] provided a method for analyzing the macula's edema using uncalibrated multiple-view fundus images. It also uses automatic algorithms to quantify features from the reconstructed image. These algorithms are helpful in the automated point-of-care identification of early macular edema, such as before the development of exudation. The method is broken down into three sections: first, a preprocessing method is used to simultaneously improve the macula's dark microstructures; second, non-morphological sparse features are used to register all available views; and third, a statistical merged to create a naive height map of the macula. The flaw of this method is it's not able to accurately determine depth. Rapantzikoset al. [12] explored the issue of automatic AMD evaluation in this research using methods based on histograms. It evaluates a histogram-based enhancement method that segments areas that differ slightly from their background regions using a histogram-based segmentation methodology and employs histogram equalization as its main operator. The inability of this method is that it is tested with only a few images.

Giancardo et al. [13] provided a collection of features based on color, wavelet decomposition, and automatic lesion segmentation for DME diagnosis. By using these features, a classifier is trained to automatically detect DME when exudation is present. This method is based on an algorithm that can identify exudates with a given confidence level without the need for machine learning techniques. The disfavor of this method is high time complexity. Akram et al. [14] offered an automated technique for detecting and classifying macular edema using an intelligence system. The method comprises a classifier based on the Gaussian mixtures model and a detailed feature set, for precise macula detection. Additionally, for better exudate detection

a hybrid classifier is used. The failure of this method is the undesired result for certain images. Mookiah et al. [15] exposed an automated fundus image-based screening technique for dry AMD. This study included various kinds of entropies, Gabor wavelet features taken from greyscale fundus images, Fractional Dimension (FD), and Higher Order Spectra (HOS) bispectra features. Using HOS and Gabor wavelet, non-linear characteristics can be recovered to identify sudden changes in both normal and dry AMD images. The negative side of this method is the difficulty in real-time implementation. Alais et al. [16] revealed a segmentation technique that evaluates the quality of retinal images with respect to the macular region's visibility. The macular region is segmented using a fully convolutional network. This algorithm can identify the fovea within an average of 0.1 mm of human performance. This method's flaw is the low image quality.

Li et al. [17] demonstrated the AMD-Net, a U-Net architecture that can partition the subretinal fluid and hemorrhage lesions of the wet AMD from the ocular fundus images. Three parts are included in the AMD-Net: the Decoder Attention Block (DAB), SKip connection Block (SKB), and Encoder Feature Fusion Unit (EFFU). The multi-scale characteristics are extracted and fused by the AMD-Net using the EFFU. Additionally, the attention module allows the EFFU to give discriminative features a larger weight. An SKB is designed by AMD-Net to lessen the semantic gap between encoder and decoder characteristics. The DAB module is based on the UNet 3+ decoder. The failure of this method is high computational cost. Wan et al. [18] exposed a combined transformer and a convolutional neural network (CSPDarknet53) to generate a hybrid model called HCSP-Net. This hybrid model was used to tri-classify color fundus photography into three categories based on clinical classification manifestations: Normal Macula (NM), Dry Macular Degeneration (DMD), and Wet Macular Degeneration (WMD). The failure of this work is its data pre-processing results were not up to the mark and it resulted in inaccurate detection.

Floriano et al. [19] exposed the mathematical morphology, DIP, and a Supporting Vector Machine (SVM) scheme for the AMD diagnosis using the fundus images. Pattern recognition algorithms are used to automatically detect the AMD region. It is accomplished by automatically creating a feature vector from the binarized fundus image's attributes. This feature vector is then supplied to an SVM classifier, which automatically identifies the patient's AMD by detecting the presence of drusen in the retina. The imperfection of this work is the inefficiency of a large quantity of macular degenerated regions. Xu et al. [20] presented the DeepDrAMD method, which is a transformer-based deep learning model for hierarchical vision that uses Color Fundus Photos (CFPs) to identify AMD. It differentiates various subtypes by integrating data augmentation techniques and Swin-Transformer. The implementation of DeepDrAMD in clinical practice can contribute to early intervention, personalized patient care, and improved outcomes in AMD management. The unworthy of this method is that it needs the careful alteration of hard-thresholds regarding real-world clinical settings. El-Khalek et al. [21] offered a thorough Computer-Aided Diagnostic (CAD) framework for classifying fundus images into four groups: normal, wet AMD, intermediate AMD, and Geographic Atrophy (GA). The minus side of this work is that it has not support for long-term follow-up of AMD.

## 3. Proposed Methodology

This research proposes a novel method for essential AMD diagnosis entitled ‘Macular Degeneration Diagnosis using OLQCT preprocessing, Fuzzy segmentation, and BPN classifier (MDD_OFB)’. It is constructed based on 3 core subjects viz. (i) Preprocessing using OLQCT method, (ii) Fuzzy-based segmentation, and (iii) Back Propagation Neural (BPN) network classifier.
The three main modules of the proposed MDD_OFB method are (i) Query fundus image feature extraction, (ii) Training process using AMD and non-AMD samples, and (iii) BPN classifier-based AMD diagnosis. The overall block diagram of the proposed MDD_OFB method is illustrated in Figure 1.

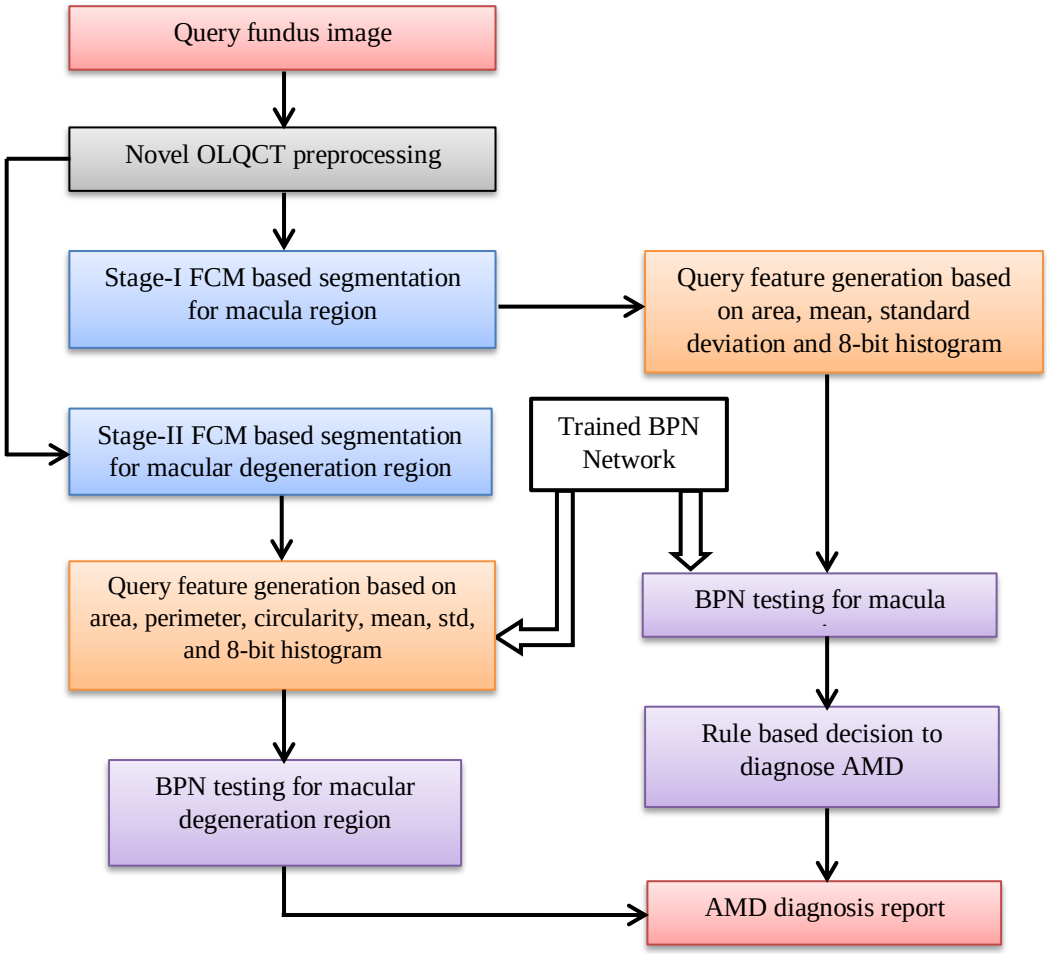


**Fig.1: Block diagram for macular degeneration diagnosis in the proposed MDD_OFB method.**

The RGB color fundus image of 24-bit format with 512x512 dimension is given as query or input to the proposed MDD_OFB method to diagnose the age-related macular degeneration disease. The novel OLQCT preprocessing method is employed to enhance the fundus image which removes the background and OD region. In this research, the dual-stage Fuzzy C Means (FCM) method is used to segment both the macula region and macular degeneration region. The Query features regarding to macula region are extracted from the macula region segmentation output of stage-I FCM. The Query features regarding to macular degeneration region are extracted from the stage-II FCM segmentation output. Both the feature sets undergo the testing process of the BPN classifier. Finally, a rule-based decision system detects the macular degeneration disease.

### 3.1 Query fundus image feature extraction

The Query fundus image is fed as input to the proposed MDD_OFB method. In this section, the process of query feature extraction is described in detail. The main modules of this process are:

- OLQCT preprocessing
- Dual stage fuzzy c means segmentation integrated with both macula region segmentation and Wet Macular segmentation
- Feature extraction.

### 3.1.1 OLQCT preprocessing

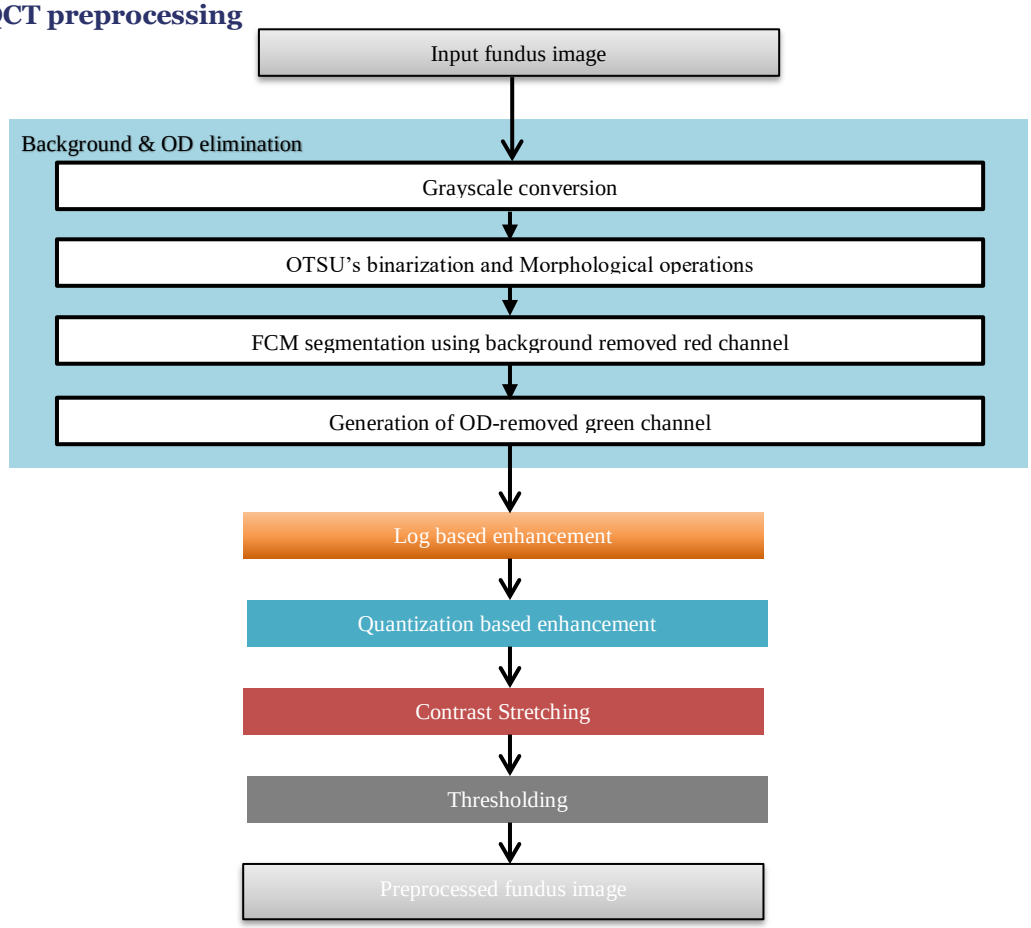


In this process, first, the novel OLQCT method is employed to preprocess the query fundus image. It removes the background and OD region in the fundus image. The general block diagram of the proposed OLQCT preprocessing method is illustrated in Figure 2. Also, Figure 3 depicts the various steps of the OLQCT preprocessing method.

**Fig.2: Block diagram for the proposed OLQCT preprocessing method.**

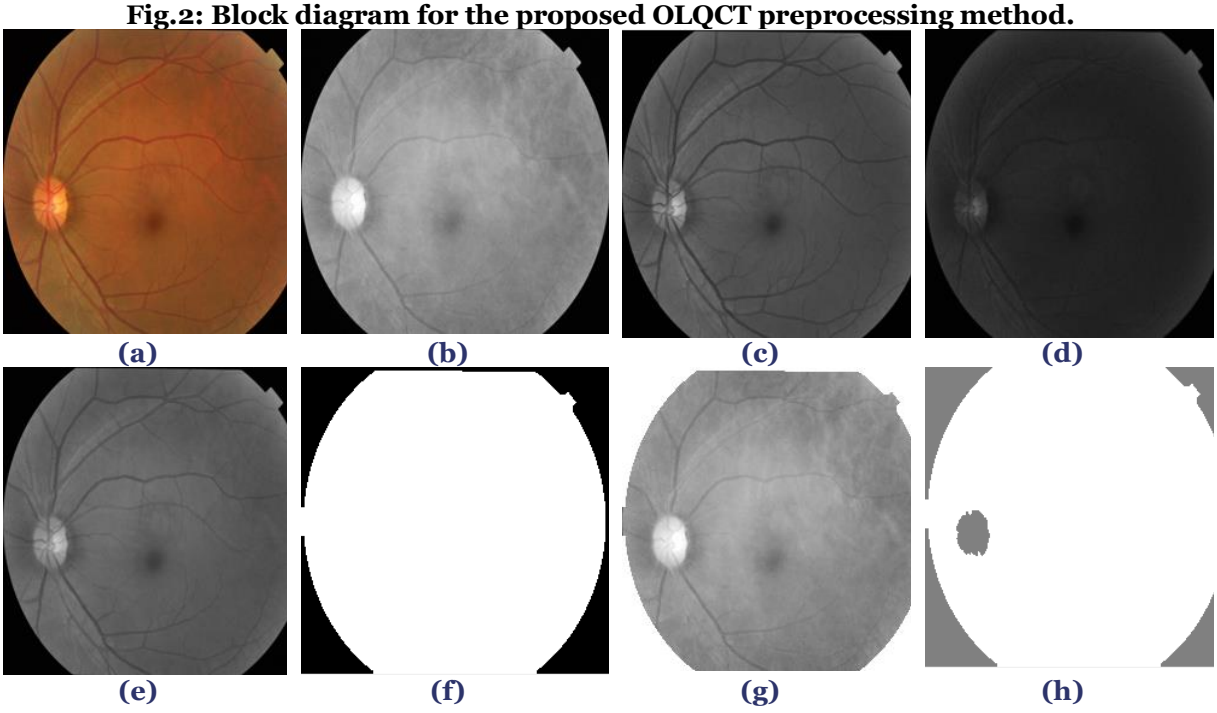

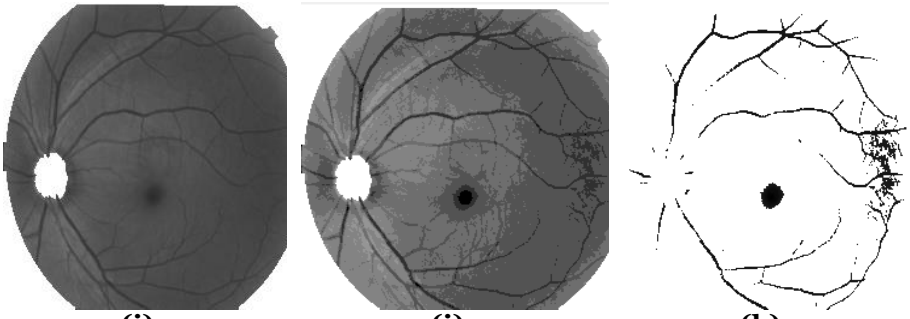

**(i) (j) (k)**

**Fig.3: Background removal process in query fundus image, (a) query image, (b) red image, (c) green image, (d) blue image, (e) grayscale image, (f) Otsus and morphological based background removed binary image, (g) foreground only red image, (h) FCM based OD segmentation, (i) OD subtracted fundus image, (j) log, quantization, contrast stretching based foreground preprocessing, (k) thresholding-based macula region preprocessing.**

The query image is read-out and stored in $I_{IP}$ image, which is shown in Figure 3(a). The red, green, and blue components of the RGB color query image $I_{IP,}$ are extracted and stored in images such as $I_R$, $I_G$, and $I_B$ respectively. Figure 3(b) depicts the red channel and Figure 3(c) shows the green channel. Figure 3(d) shows the blue channel image. Next, the grayscale conversion process is forwarded to get the single-channel grayscale image $I_{GS}$ instead of the multichannel RGB image $I_{IP}$, based on Equation (1). The output of the grayscale image is shown in Figure 3(e).

The binarization process proceeds to segment the background region using OTSUS- binarization method. OTSUS-binarization is referred to in Otsus (1979). It computes a global threshold from the grayscale image $I_{GS}$. It chooses a threshold T that minimizes the intraclass variance of the thresholded black and white pixels. The selected threshold is used to binarize the fundus image using Equation (1).

$$I_{BIN}^{i,j} = \{1, if\ I_{GS}^{i,j} > T\ \ 0,\ else \quad (1)$$

$$i \in [0, H-1], j \in [0, W-1]$$

Herein, the term $I_{BIN}$ refers to the binarized image, $T$ refers to the Otsu threshold, $H$ refers to the height of the image, and $W$ refers to the width of the image.

The binarized image contains many small holes, and they are removed using morphological processing. A structuring element SE of square shape with $3 \times 3$ dimension is generated. Normally, the binary image $I_{BIN}$ contains a ring structure in the outer region of the foreground. It interrupts the upcoming processes. Hence, it should be removed. The erosion operation of the morphological approach is employed twice using the structural element SE. This background-removed binary image is noted as $I_{BIN}$ and it is shown in Figure 3(f). Herein, the background is represented by zeros, while the foreground is represented by ones.

Optic Disc (OD) is one of the main components in the fundus image. It refers to the optic nerve region. This OD region appears as an obstacle when segmenting the macula region. Therefore, the macula region segmentation process needs the elimination or absence of the OD region, which promotes or enhances the quality of upcoming macula region and macular region segmentation. The OD segmentation is much supported by the red color channel, hence, the background removed the red color channel $I_{BR}$ is obtained using Equation (2).

$$I_{BR}^{i,j} = \{I_R^{i,j}, if\ I_{BIN}^{i,j} = 1\ \ 255,\ else \quad (2)$$

The $I_{BR}^{i,j}$ pixel location receives the real values of $[i,j]^{th}$ location of $I_R$ image when regarding to foreground region, and for the background region it receives 255 which corresponds to white color. The color of the macula or macular region is related to dark color, and it coincides with the dark color of the background region. This contradiction negatively impacts the upcoming macula or macular region segmentation. Suppose, the background region is filled with other-than-dark colors, then it will increase the quality of both macula and macular region segmentation. Hence, the bright intensity value 255 is chosen to fill the background region in the red channel. Figure 3(g) shows the output of the background removed red channel image.

Fuzzy C Means is the fuzzy-based segmentation method that segments the image into k meaningful groups in an unsupervised manner. The background removed the red image $I_{BR}$ is given as input to the FCM process. It segments the image into two groups. The first group denotes the background and the OD region, whereas the second group denotes the foreground region except the OD region. Meaning that, the 'background and the OD region' is represented by a single unique number, and the foreground region is marked by another single unique number. The [0,0]th pixel in the segmented image indicates the numeric value of the OD region and the background region. The FCM segmentation output is noted as $I_{SEG}$, which is shown in Figure 3(h). The background removed the green image $I_{BG}$ is obtained similar to $I_{BR}$. The OD eliminated the green image $I_{ODG}$ is obtained using the aid of $I_{SEG}$ image and the $I_{BIN}$ image, which is guided by Equation (3).

$$I_{ODG}^{i,j} = \{255, if\ I_{BIN}^{i,j} = 1\ \&\ I_{SEG}^{i,j} = I_{SEG}^{0,0}\ \ I_{BG}^{i,j},\ else \quad (3)$$

$$i \in [0, H-1], j \in [0, W-1]$$

In Equation (3), the term $I_{SEG}^{0,0}$ refers to the value of $[0,0]^{th}$ pixel of $I_{SEG}$ image. The resultant background and OD eliminated the green image $I_{ODG}$ is shown in Figure 3(i), where both background and OD regions are marked by 255. The $I_{ODG}$ image is further enhanced by a *log*-based approach using Equation (4).

$$I_{ODG} = log_{10}(I_{ODG}) \quad (4)$$

In Equation (4), the image is enhanced by a logarithmic way that suppresses the background while improving the macula region or the macular region. A uniform quantization is approached to limit the values in a smaller level, using Equation (5).

$$I_{ODG} = \frac{I_{ODG}}{QC} \quad (5)$$

In Equation (5), the term $QC$ refers to the quantization constant, which is fixed as 12. This constant yields a smooth region that supports better image enhancement. The contrast stretching process is employed to improve the contrast level, using Equation (6).

$$I_{ODG} = I_{ODG} - min(I_{ODG}) \quad (6)$$

Equation (6) ensures the starting intensity of the enhanced image as 0. It stretches the intensity range to a better level. Further, the range of intensity is extended to 0 to 255 using Equation (7).

$$I_{ODG} = fix\left(\frac{I_{ODG}}{max(I_{ODG})} \times 255\right) \quad (7)$$

Herein, the term $\frac{I_{ODG}}{max(I_{ODG})}$ yields the data range from 0 to 1.0. The constant 255 stretches the contrast to the complete-intensity range that is 0 to 255. Figure 3(j) illustrates the output of the enhanced version. The $I_{ODG}$ image is thresholded based on the constant $th$ using Equation (8).

$$I_{OLQCT}^{i,j} = \{255,\ if\ I_{ODG}^{i,j} > th\ I_{ODG}^{i,j}, else \quad (8)$$

In Equation (8), the term $I_{OLQCT}$ expresses the enhanced image by the proposed OLQCT preprocessing method. The threshold $th$ is fixed as 64 which is decided based on multi-trials in this experiment. The output of $I_{OLQCT}$ is shown in Figure 3(k), which contains the macula region as well as some other vessel components, but not the background, inner tissue, and OD. This enhanced result supports the upcoming segmentation tasks.

### 3.1.2 Dual stage fuzzy c means segmentation integrated with both macula region segmentation and Wet Macular segmentation

In this section, the macula region and the wet macular region are segmented individually based on the FCM process. The FCM clustering algorithm works based on fuzzy technology and it clusters the given image into C meaningful clusters. This section deals with the concept of dual FCMs that belongs to two stages of segmentation. The first stage of segmentation is related to the macula region segmentation and the second stage is related to the wet macular region segmentation.

In the first stage, FCM accepts the preprocessed $I_{OLQCT}$ image as input and delivers the output of macula region segmentation. The FCM is configured as below to get an effective segmentation:

- Total clusters = 4
- Exponent value = 2
- Maximum iterations = 100
- Minimum improvement =1.

There is a possibility of the regions such as background, low contrast tissue area, high contrast tissue area, and macula area. Hence, Total clusters are fixed as 4. The initial process starts with the objective function, membership matrix, center computation, etc. Afterwards, the distance computation and membership updation processes are performed. Finally, the objective function decides the quitting of the FCM loop, and the defuzzification process constructs the segmented image. Figure 4(a) shows the segmented results of FCM. The segmented image contains four binary images, each containing an individual cluster among the four clusters. Those binary images are marked as $I_{BIN1,}$ $I_{BIN2,}$ $I_{BIN3,}$ and $I_{BIN4.}$ The mean computation process is employed on the $I_{BIN1}$ binary image based on Equation (9).

$$\mu = \frac{\sum_{i=0}^{H-1} \sum_{j=0}^{W-1} f(I_{BIN1}^{i,j})}{\sum_{i=0}^{H-1} \sum_{j=0}^{W-1} I_{BIN1}^{i,j}} \quad (9)$$

$$f(I_{BIN1}^{i,j}) = \{I_{OLQCT,}^{i,j}\ if\ I_{BIN1}^{i,j} = 1\ \ 0, \quad else \quad (10)$$

where

$\mu_2$ – Mean of intensities corresponding to $I_{BIN1}$ image

$f(x)$ – Function to retrieve intensity data

In Equation (10), the mean value is computed on the locations of 1s in the $I_{BIN1}$ image. Similar to this, the $\mu_2, \mu_3$ and $\mu_4$ are computed based on the $I_{BIN2,}$ $I_{BIN3,}$ and $I_{BIN4}$ images. Also, the minimum mean value $\mu$ is computed. The minimum $\mu$ provider's index is found, and based on that the corresponding binary image is chosen as the binary version of the segmented image. From this image, the maximum-area object is found and it is noted as the binary version of the macula region segmented image $I_{BIN\_MR}$.

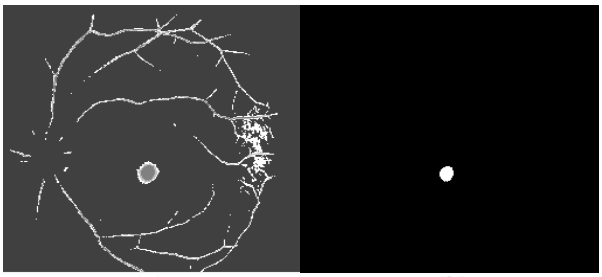

**(a) (b)**

**Fig. 4: First stage segmentation results, (a) FCM based clustering, (b) macula region segmented image.**

The $I_{BIN\_MR}$ image's locations corresponding to 1s are undergone to generate the intensity version of macula region segmentation using the Green image $I_G$. The locations of 0's of $I_{BIN\_MR}$ image loaded with the values of 25. It can be shown in Equation (11).

$$I_{MRS}^{i,j} = \{I_G^{i,j}, \ if\ I_{BIN\_MR}^{i,j} = 1\ 255, \ else \quad i \in [0, H-1], j \in [0, W-1] \tag{11}$$

In Equation (11), the term $I_{MRS}$ refers to the macula region segmented image. The macula region segmented image is explored in Figure 4(b).

The second stage performs the FCM segmentation for wet macular region segmentation. It accepts the grayscale image $I_{GS}$ as input and delivers the output of wet macular region segmented image. The FCM segmentation is applied similar to the previous model segmentation for the $I_{GS}$ image with the same configuration. The output of FCM segmentation is depicted in Figure 5(a). It yields four binary images. The corresponding four mean values are computed similar to Equation (9). The minimum mean $\mu$ is computed. The corresponding cluster regarding $\mu$ is found, and that binary cluster image is employed for two morphological operations such as erosion followed by dilation to disconnect the unwanted small connections with neighbour objects. The maximum-area object is used to construct the binary version of wet macular region segmentation which is noted as $I_{BIN\_WMR.}$

The intensity version of the wet macular region is obtained using $I_{BIN\_WMR}$ image and grayscale image $I_{GS}$ using Equation (12).

$$I_{WMRS}^{i,j} = \{I_{GS}^{i,j}, \ if\ I_{BIN\_WMR}^{i,j} = 1\ 255, \ else \quad i \in [0, H-1], j \in [0, W-1] \tag{12}$$

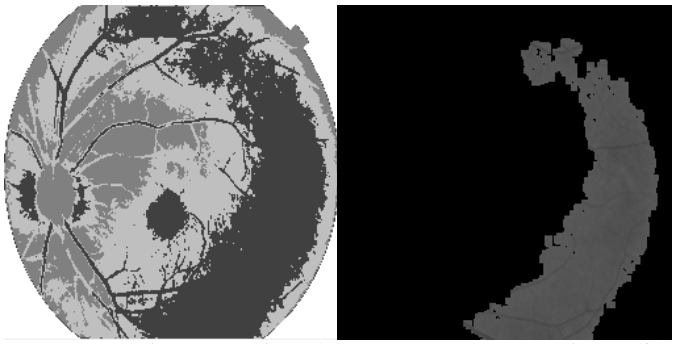

**Fig. 5: Second stage segmentation results, (a) FCM segmentation, (b) wet macular region segmentation output.**

In Equation (12), the term $I_{WMRS}$ refers to the wet macular region segmented image. Herein, the wet macular region is indicated by the intensities derived from the grayscale image while the other pixels are fixed 255. The output of $I_{WMRS}$ image is shown in Figure 5(b). The FCM process regarding to macular region is exactly tuned to segment the wet macular region only and it is not suitable for the macula region. Herein, the input image is a non-AMD image, i.e. it contains only the macula region and not the wet macular degeneration region. This current FCM process falsely detects the macular degeneration area, because in this image the AMD region is absent. If suppose, there is the possibility of AMD region, then the proposed approach exactly detects the AMD region. But, in this current experiment, it is not possible. Shortly speaking, the macula region supporting FCM (i.e. stage-1 FCM) detects macula region exactly and not the macular region. Also, the macular region supporting FCM (i.e. stage-2 FCM) detects the macular region exactly and not the macula region. Hence, in Figure 5(b) it is an irrelevant one regarding to AMD region. Thus, the Dual FCM system segments both the macula region and the wet macular region.

### 3.1.3 Feature extraction

This section extracts the feature data from the cropped regions of both macula segmentation and macular segmentation. It extracts thirteen effective features for the query fundus image. They are:

- Area property
- Perimeter property
- Circularity property
- Mean property
- Standard Deviation (STD) property
- Eight-bin histogram.

Area property refers the measure of area occupied by the segmented object, which is measured using the bounding box of binary cropped object. Perimeter is the property that is the measure of the contour of object which is measured using the binary cropped object. Circularity property is the measure of circular-form of the binary cropped object. The mean-property refers the average intensity of the cropped segmented object. The STD property reflects the variation level of the cropped object. Eight-bin histogram reflects the frequency of intensity values that are compressed in eight bins.

The binary macula segmented image $I_{BIN\_MR}$ is processed to get the bounding box of the macula object. Also, the intensity data corresponding to bounding box is extracted from the $I_{GS}$ image. The binary bounding box object is noted as $I_{BBox}$. The Gray bounding box object is noted as $I_{GS\_Box}$. The area, perimeter and circulatiy features are computed from the $I_{BBox}$ image and stored as query macula region features such as $F^0_{Q\_MR,}$ $F^1_{Q\_MR,}$ and $F^2_{Q\_MR,}$ respectively. The mean features, and STD features are computed from the $I_{GS\_Box}$ object, and stored in $F^3_{Q\_MR}$ and $F^4_{Q\_MR}$ respectively. The histogram of $I_{GS\_Box}$ is found along with 8 bins, and it is stored as in the range of features from $F^5_{Q\_MR}$ and $F^{12}_{Q\_MR}$. The total feature corresponding to macula region is 13. In the similar manner, the Query wet macular region features are found and stored in the range of features from $F^0_{Q\_WMR}$ to $F^{12}_{Q\_WMR}$. Thus, the macula region and wet macular region-based features are computed.

## 3.2 Training process using non-AMD and AMD samples

Training a neural network means training sample feature vectors using a learning process to get a trained network that can able to do a classification task. In this section, $m$ samples from non-AMD and $n$ samples from AMD are collected from a dataset, and they are used to train the neural network. The block diagram of the training process is explored in Figure 6.

BPN is a type of Artificial Neural Network (ANN) that utilizes the back-propagation algorithm for training. It is widely used for supervised learning tasks, particularly in classification tasks. It consists of multiple layers, and they are:

- Input layer
- Hidden layer
- Output layer.

The input layer receives input features, and the hidden layer performs computations using activation functions. The output layer delivers the final predicted result. The BPN algorithm is a supervised learning technique used to minimize the error between actual and predicted outputs. It does the below steps:

- Forward propagation
- Error calculation
- Backward propagation
- Weight update.

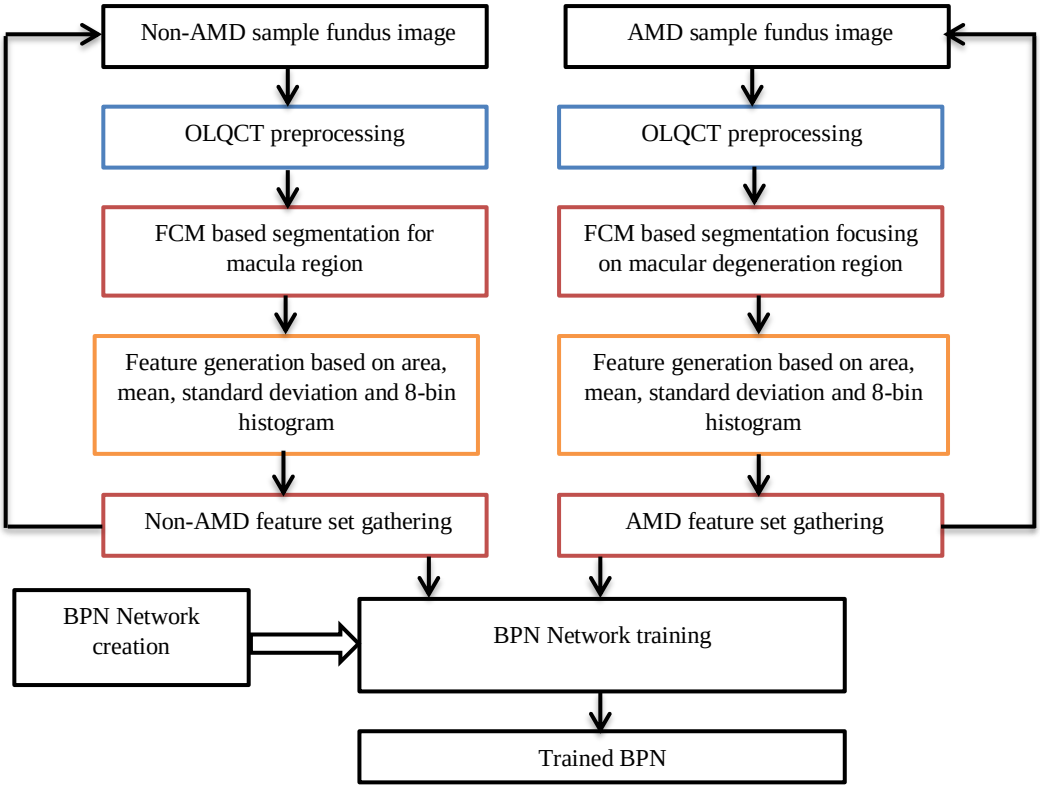


**Fig. 6: Block diagram for the training process in the proposed MDD_OFB method.**

In the first step, inputs are passed through the network, and the outputs are computed. In the second step, the difference between actual and predicted outputs is calculated using a loss function. In the third step, the error is propagated backward through the network using gradient descent to adjust the weights. In the final step, the weights are updated using the gradient of the loss function to reduce error. BPN network can model complex patterns and relationships. It works well for large datasets. BPN is a powerful tool to perform image recognition, financial forecasting, and medical image classification.

The $m$ samples of non-AMD type undergone the feature extraction process similar to query processing, and they are noted as $F_{D\_MR}^{p,q}$, where $p \in [0, m-1], q \in [0,12]$. The $n$ samples of AMD type undergone the feature extraction process similar to query processing, and they are noted as $F_{D\_WMR}^{p,q}$, where $p \in [0, n-1], q \in [0,12]$.

The BPN network is configured with learning rate=0.0001, momentum constant=0.0009, maximum iterations=100, and goal=0.00000008. The targets or known-outputs are set to non-AMD features as '0' which AMD features keep it as '1'.

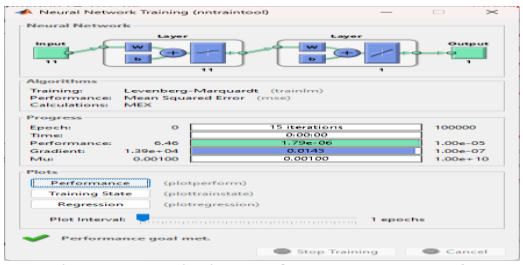


**Fig. 7: Training of BPN network.**

The training process is invoked using the arguments like BPN network, training feature vectors that contain both the macular region and wet macular region, and target vector to get the predicts output. Figure 7 shows the training process of features. The trained-BPN network is noted as BPN-net.

### 3.3 BPN classifier-based AMD diagnosis

In this section, the query feature set corresponding to the macula region (i.e., $F_{Q\_MR}$) is tested using the trained-BPN network based on MATLAB's built-in command 'sim()' along with the parameters such as BPN-net and $F_{Q\_MR}$. The predicted value is noted as $\beta$. Also, the query feature set $F_{D\_WMR}$ corresponding to the wet macular region is tested using the trained-BPN network. The predicted value is noted as $\gamma$.

A rule-based system is designed to detect/classify macular degeneration disease which incorporates both parameters $\beta$ and $\gamma$. The decision system is given in Equation (13), Equation (14), and Equation (15).

$$\delta_{MR} = |0 - \beta| \quad (13)$$

$$\delta_{WMR} = |1 - \gamma| \quad (14)$$

$$\rho = \{1, if\ \delta_{MR} < \delta_{WMR}\ \ 0, else \quad (15)$$

In Equation (13), the term $\delta_{MR}$ refers to the measure of closeness against the constant '0'. In Equation (14), the term $\delta_{WMR}$ refers to the measure of closeness against the constant '1'. Herein, the constant '0' refers to the target value corresponding to non-AMD, and the constant '1' refers to the target value corresponding to AMD disease. In Equation (13), the error in non-AMD based prediction is computed while in Equation (14), the error in AMD based prediction is computed. In Equation (15), the minimum value among $\delta_{MR}$ and $\delta_{WMR}$ are found. If $\delta_{MR}$ is the minimum value, then '1' is returned, otherwise 0 is returned. The term $\rho$ means the final prediction result.

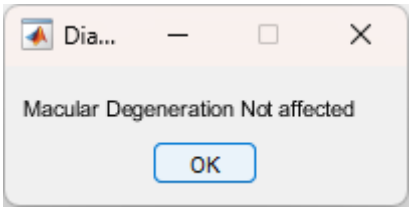


**Fig. 8: AMD diagnosis report.**

If $\rho$ is equal to 1 then the given image is reported as non-AMD, otherwise it is reported as AMD. Figure 8 shows the report of AMD diagnosis. Thus, the classification process successfully diagnoses the AMD disease.

## 4. Experimental Results

This research considers three methods regarding macular degeneration to make the analysis against the proposed MDD_OFB method. They are:

- Macular Degeneration diagnosis using Machine Learning (MD_ML) [19]
- Macular Degeneration diagnosis using Deep Learning with Hierarchical Vision Transformer (MD_DLHVT) [20]
- Macular Degeneration diagnosis using Machine Learning based Classification (MD_MLC) [21].

The proposed AMD diagnosis method uses three image datasets, and they are:

- Kaggle Fundus Image Database (KFI_DB) [22]
- STructured Analysis of the REtina Database (STARE_DB) [23]
- Retinal Fundus Multi-disease Image Database (RFMI_DB) [24].

The databases namely, KFI_DB, STARE_DB, and RFMI_DB contain the fundus images that belongs to normal and abnormal referred with wet macular degeneration. Five analytic measures are used to assess the effectiveness of the proposed MDD_OFB method, and they are: Precision, Accuracy, Dice Coefficient, Time taken, and Confusion matrix.

Precision is a metric used to determine the classification performance of an algorithm. It can be defined in Equation (18).

$$Precision = \frac{Correctly\ classified\ actual\ positives}{Everything\ classified\ as\ positive} \quad (18)$$

The range of data that is fixed in this analysis is from 0 to 1. The high precision means better classification and vice versa. In this analysis, 300 test images per database, are randomly selected for evaluating the AMD diagnosis algorithms.

**Table 1: Average Precision analysis for AMD diagnosis**

| Database | Average Precision | | | |
|---|---|---|---|---|
| | Methods | | | |
| | MD_ML | MD_DLHVT | MD_MLC | Proposed MDD_OFB |
| KFI_DB | 0.940 | 0.943 | 0.972 | **0.984** |
| STARE_DB | 0.920 | 0.928 | 0.970 | **0.980** |
| RFMI_DB | 0.944 | 0.952 | 0.972 | **0.988** |

Accuracy is an analytic measure that is used to measure the performance of the classification algorithms. It is the proportion of all classifications that are correct, whether positive or negative. It can be computed using Equation (19).

$$Accuracy = \frac{Correct\ classifications}{Total\ classifications} \quad (19)$$

The higher accuracy refers to better classification. Herein, 300 test images in each database are chosen, and they are used to analyze the proposed MDD_OFB method against the existing methods

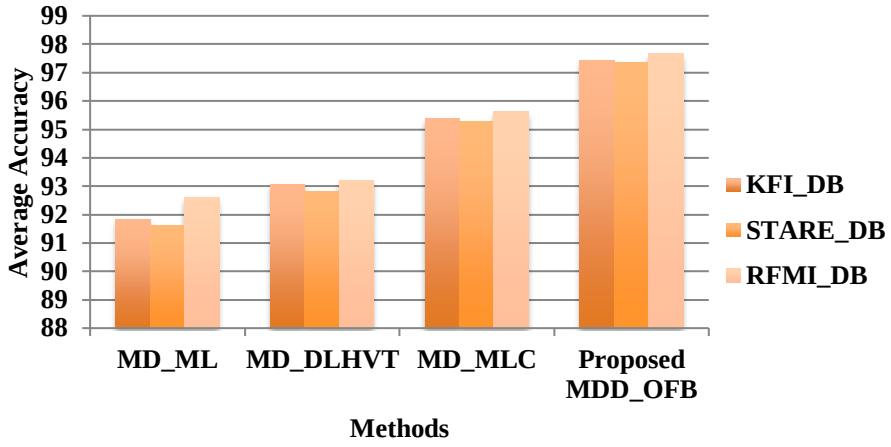


**Fig. 9: Average Accuracy analysis chart for AMD diagnosis.**

Dice Coefficient analysis on AMD diagnosis determines the classification power of the proposed method and the other existing methods. It compares the pixel-wise agreement between a predicted classification and its corresponding ground truth. It is computed based on Equation (20).

$$DC = \frac{2\times|X\cap Y|}{|X|+|Y|} \quad (20)$$

Herein, the term $DC$ means the Dice Coefficient. It occupies the data range between 0 to 1. In Equation (20), the term X means predicted results and Y is the ground truth. The higher dice score shows the better performance of a specified classification algorithm.

**Table 2: Average Dice Coefficient analysis for AMD diagnosis**

| Database | Average Dice Coefficient | | | |
|---|---|---|---|---|
| | Methods | | | |
| | MD_ML | MD_DLHVT | MD_MLC | Proposed MDD_OFB |
| KFI_DB | 0.9090 | 0.9216 | 0.9448 | **0.9652** |
| STARE_DB | 0.9051 | 0.9170 | 0.9416 | **0.9645** |
| RFMI_DB | 0.9171 | 0.9230 | 0.9471 | **0.967**4 |

In AMD diagnosis, the Time Taken metric measures the overall amount of time needed for a patient to obtain a verified diagnosis. The unit of this metric is known as 'seconds'.

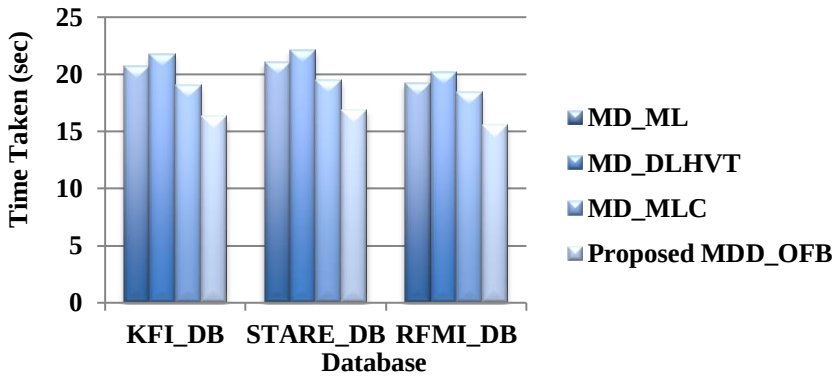


**Fig.10: Average Time taken analysis for AMD diagnosis.**

The Confusion Matrix is a crucial tool for evaluating the accuracy of diagnostic algorithms in detecting AMD. It compares the model's predictions to the actual results to give a thorough analysis. False Positives (FP), True Negatives (TN), False Negatives (FN), and True Positives (TP) are the four main parts of the matrix used in AMD diagnosis. True Positives are AMD cases that were accurately identified, whereas False Negatives are AMD cases that the model failed to detect. False Positives are non-AMD cases that are misdiagnosed as AMD, while True Negatives are non-AMD cases that are accurately categorized as negative. In this analysis, 500 test images are chosen randomly from each of the three datasets such as KFI_DB, STARE_DB, and RFMI_DB to evaluate the performance of the proposed method and existing methods.

| | Predicted Positive (P) | Predicted Negative (N) |
|---|---|---|
| **Actual Positive (P)** | TP=238 | FN=25 |
| **Actual Negative (N)** | FP=12 | TN=225 |

(a)

| | Predicted Positive (P) | Predicted Negative (N) |
|---|---|---|
| **Actual Positive (P)** | TP=227 | FN=11 |
| **Actual Negative (N)** | FP=23 | TN=239 |

(b)

| | Predicted Positive (P) | Predicted Negative (N) |
|---|---|---|
| **Actual Positive (P)** | TP=244 | FN=16 |
| **Actual Negative (N)** | FP=6 | TN=234 |

| | Predicted Positive (P) | Predicted Negative (N) |
|---|---|---|
| **Actual Positive (P)** | TP=246 | FN=8 |
| **Actual Negative (N)** | FP=4 | TN=242 |

**Fig.11: Confusion matrices for the AMD diagnosis using four methods for RFMI_DB database; (a) MD_ML method, (b) MD_DLHVT method, (c) MD_MLC method, (d) proposed MDD_OFB method.**

## 5. Discussion

Table 1 describes the analytic results based on precision metric. The 'wet macular degeneration affected images' and 'non-affected images' are given for precision-based classification analysis on four AMD diagnosis methods such as MD_ML, MD_DLHVT, MD_MLC, and the proposed MDD_OFB to evaluate this assessment. The three effective databases KFI_DB, STARE_DB, and RFMI_DB are used to make this analysis an essential one. The RFMI_DB database reaches the best performance (i.e., 0.988) because it attains the highest average-precision result. The overall-precision results corresponding to the four methods are 0.934, 0.941, 0.971, and 0.984, with respect to MD_ML, MD_DLHVT, MD_MLC, and the proposed MDD_OFB methods. The proposed method produces the highest overall-precision result, i.e., 0.984, therefore it produces better precision than the existing methods. The MD_MLC method is noted as the second-best method, because it produces the second-grade overall-precision value i.e., 0.971. This analysis proves that the proposed method is better than the existing methods.

Figure 9 reveals the analysis that is based on the average accuracy of AMD diagnosis or classification. The affected and non-affected image samples of macular degeneration are used for this assessment. The average accuracy of the proposed method regarding the three databases such as KFI_DB, STARE_DB, and RFMI_DB are 97.436, 97.366, and 97.659. These values explore that the proposed method yields higher accuracy than the existing methods, irrespective of the databases. The RFMI-DB database supports essentially for the AMD diagnosis than the other two databases. The overall accuracies of the four methods such as MD_ML, MD_DLHVT, MD_MLC, and the proposed MDD_OFB are 92.006, 93.032, 95.431, and 97.487. This analysis proves that the proposed method improves the accuracy regarding to AMD diagnosis.

Dice Coefficient analysis for the AMD diagnosis is shown in Table 2 for the three existing methods and the proposed MDD_OFB method. The dice coefficient of the MDD_OFB method has the highest value of 0.9674 which corresponds to the RFMI_DB database. The MDD_OFB method is the best method for diagnosing AMD among the three methods. As per this study, the MD_MLC method is the second-best method for AMD diagnosis because it yields the range of dice coefficients from 0.9416 to 0.9471, which are less than the proposed MDD_OFB and greater than both the MD_ML and MD_DLHVT methods. Finally, the MD_ML method yields the lowest dice coefficient for AMD diagnosis. The proposed MDD_OFB method is the winner among the four methods based on the Dice coefficient metric.

The Time-Taken analysis compares the proposed MDD_OFB method with three existing methods for AMD diagnosis, as illustrated in Figure 10. The MDD_OFB method demonstrates the shortest time by taking 15.57 seconds on the RFMI_DB dataset, which makes it the fastest approach for AMD diagnosis. For the other two datasets such as KFI_DB and STARE_DB, the MDD_OFB method records the minimal times of 16.32 seconds and 16.90 seconds, respectively. Conversely, the existing MD_DLHVT method is the slowest, with a maximum time of 22.13 seconds for diagnosing AMD.

Figure 11 shows the four confusion matrices related to the four methods including MD_ML, MD_DLHVT, MD_MLC, and the proposed MDD_OFB database. Figure 11(a) shows the confusion matrix related to the MD_ML method. Figure 11(b) denotes the confusion matrix regarding the MD_DLHVT method. Figure 11(c) focuses on the confusion matrix of the MD_MLC method, and Figure 11(d) depicts the confusion matrix of the proposed MDD_OFB method. The proposed MDD_OFB method yields the highest TP of 246, meanwhile, it yields the least FP when compared to existing methods. Also, the proposed method delivers the highest TN of 242, and the least FN of 8 while compared with the existing versions of AMD diagnosis. The MD_MLC method activates as the second-best method because according to the confusion matrix specified in Figure 11(c), it delivers secondary-level better results for the four parameters such as TP, FP, TN, and FN. The MD_ML method is the least performer according to its confusion matrix. This analysis proves that the proposed MDD_OFB method acts as the highly best approach for AMD diagnosis in fundus images.

## 6. Conclusion

The MDD_OFB method is proposed for diagnosing AMD in fundus images which integrates OLQCT preprocessing, FCM segmentation, and a BPN classifier algorithm. The innovative OLQCT preprocessing technique improves fundus images by eliminating the background and OD region. A dual-stage FCM approach is used to segment both the macula and macular degeneration regions. Features from the macula region are extracted from the Stage-I FCM output, while features from the macular degeneration region come from Stage-II FCM. These feature sets are then tested with the BPN classifier. The method's performance in diagnosing AMD is assessed using databases like KFI_DB, STARE_DB, and RFMI_DB. Results show that the MDD_OFB method outperforms others, achieving the highest precision, accuracy, and dice coefficient, along with fast execution across all datasets. It improves accuracy by 2.056%, increases the dice coefficient by 2.244, and reduces processing time by 2.743 seconds compared to the second-best MD_MLC method. Overall, the proposed MDD_OFB method demonstrates superior diagnostic performance for AMD compared to existing methods.

## References

[1] Syed A.M., Akram M.U., Akram T., Muzammal M., Khalid S., and Khan M.A., 2018, 'Fundus images-based detection and grading of macular edema using robust macula localization', IEEE access, vol. 6, pp. 58784-58793.

[2] Deng Y., Qiao L., Du M., Qu C., Wan L., Li J., and Huang L., 2022, 'Age-related macular degeneration: epidemiology, genetics, pathophysiology, diagnosis, and targeted therapy', Genes & diseases, vol. 9, issue 1, pp. 62-79.

[3] Gheorghe A., Mahdi L., and Musat O., 2015, 'Age-related macular degeneration', Romanian journal of ophthalmology, vol. 59, issue 2, pp.74-77.

[4] Morales S., Engan K., Naranjo V., and Colomer A., 2015, 'Detection of diabetic retinopathy and age-related macular degeneration from fundus images through local binary patterns and random forests', IEEE International conference on image processing (ICIP), Quebec City, QC, Canada, pp. 4838-4842.

[5] Li X., Hu X., Yu L., Zhu L., Fu C. W., and Heng P. A., 2020, 'CANet: Cross-disease attention network for joint diabetic retinopathy and diabetic macular edema grading', IEEE transactions on medical imaging, vol. 39, issue 5, pp. 1483-1493.

[6] Wang W., Li X., Xu Z., Yu W., Zhao J., Ding D., and Chen Y., 2011, 'Learning two-stream CNN for multi-modal age-related macular degeneration categorization', IEEE journal of biomedical and health informatics, vol. 26, issue 8, pp. 4111-4122.

[7] Alais R., Dokladal P., Erginay A., Figliuzzi B., and Decenciere E., 2020, 'Fast macula detection and application to retinal image quality assessment', Biomedical signal processing and control, vol. 55, pp. 1-10.

[8] Kose C., Sevik U., and Gencalioglu O., 2008, 'Automatic segmentation of age-related macular degeneration in retinal fundus images', Computers in biology and medicine, vol. 38, issue 5, pp. 611-619.

[9] Tobin K.W., Chaum E., Govindasamy V.P., and Karnowski T.P., 2007, 'Detection of anatomic structures in human retinal imagery', IEEE transactions on medical imaging, vol. 26, issue 12, pp. 1729-1739.

[10] Niemeijer M., Abramoff M.D., and Ginneken B., 2007, 'Segmentation of the optic disc, macula and vascular arch in fundus photographs', IEEE transactions on medical imaging, vol. 26, issue 1, pp. 116-127.

[11] Giancardo L., Meriaudeau F., Karnowski T.P., Tobin K.W., Grisan E., Favaro P., Ruggeri A., and Chaum E., 2011, 'Textureless macula swelling detection with multiple retinal fundus images', IEEE transactions on biomedical engineering, vol. 58, issue 3, pp. 795-799.

[12] Rapantzikos K., Zervakis M., and Balas K., 2003, 'Detection and segmentation of drusen deposits on human retina: Potential in the diagnosis of age-related macular degeneration', ELSEVIER, Medical image analysis, vol. 7, issue 1, pp. 95-108.

[13] Giancardo L., Meriaudeau F., Karnowski T.P, Li Y., Garg S., Tobin K.W., and Chaum E., 2012, 'Exudate-based diabetic macular edema detection in fundus images using publicly available datasets', ELSEVIER, Medical image analysis, vol. 16, issue 1, pp. 216-226.

[14] Akram M.U., Tariq A., Khan S.A., and Javed M.Y., 2014, 'Automated detection of exudates and macula for grading of diabetic macular edema', ELSEVIER, Computer methods and programs in biomedicine, vol. 114, issue 2, pp. 141-152,
[15] Mookiah M.R.K., Acharya U.R., Koh J.E.W., Chandran V., Chua C.K., Tan J.H., Lim C.M., Ng E.Y.K., Noronha K., Tong L., and Laude A., 2014, 'Automated diagnosis of age-related macular degeneration using greyscale features from digital fundus images', ELSEVIER, Computers in biology and medicine, vol. 53, pp. 55-64.
[16] Alais R., Dokladal P., Erginay A., Figliuzzi B., and Decenciere E., 2020, 'Fast macula detection and application to retinal image quality assessment', ELSEVIER, Biomedical signal processing and control, vol. 55, pp. 1-8.
[17] Li P., Liang L., Gao Z., and Wang X., 2023, 'AMD-Net: Automatic subretinal fluid and hemorrhage segmentation for wet age-related macular degeneration in ocular fundus images', Biomedical signal processing and control, vol. 80, Article No. 104262.
[18] Wan C., Zhao J., Hong X., Yang W., and Zhang S., 2024, 'HCSP-Net: a novel model of age-related macular degeneration classification based on color fundus photography', SPRINGER, Computers materials and continua, vol. 79, issue 1, pp. 391-407.
[19] Floriano A.G., Santiago A.F., Nieto O.C, and Marquez C.Y., 2019, 'A machine learning approach to medical image classification: detecting age-related macular degeneration in fundus images', Computers & electrical engineering, vol. 75, pp. 218-229.
[20] Xu K., Huang S., Yang Z., Zhang Y., Fang Y., Zheng G., Lin B., Zhou M., Sun J., 2023, 'Automatic detection and differential diagnosis of age-related macular degeneration from color fundus photographs using deep learning with hierarchical vision transformer', Computers in biology and medicine, vol. 167, pp. 1-11.
[21] El-Khalek A.A.A., Balaha H.M., Alghamdi N.S., Ghazal M., Khalil A.T., Abo-Elsoud M.E.A., and El-Baz A., 2024, 'A concentrated machine learning-based classification system for age-related macular degeneration (AMD) diagnosis using fundus images. Scientific reports', vol.14, issue 1, pp. 1-20.
[22] KFI-DS, 2022, Accessed from <http://www.kaggle.com/datasets/linchundasn/fundusimage1000?resource=download>, Accessed on [10-June-2022].
[23] STARE-DS, 2022, Accessed from <http://cecas.clemson.edu/~ahoover/stare/>, Accessed on [10-June-2022].
[24] Pachade S., Porwal P., Thulkar D., Kokare M., Deshmukh G., Sahasrabuddhe V., Giancardo L., Quellec G., Meriaudeau F., 2021, 'Retinal fundus multi-diseases image (RFMiD): A dataset for multi-diseases detection research', MDPI, Data, vol. 6, pp. 1-14.